## PAPER

Check for updates

# Designer DNA nanocages modulate anti-oxidative and anti-inflammatory responses in tumor associated macrophages†

Payal Vaswani and Dhiraj Bhatia 🆔 *

Cancer is a complex disease, with multiple treatment modalities, but no definitive cure. The tumor microenvironment contributes to the complexity of the disease by forming a niche of multiple cell types supporting each other to carry out various cellular functions. Tumor associated macrophages are one such kind of cells which support the tumor microenvironment *via* immunosuppression. DNA tetrahedron (TD), a widely explored DNA nanocage, has shown a lot of potential in therapeutics. However, the role of TD still remains quite unexplored in immunology. Here, we first establish the anti-oxidative and anti-inflammatory role of TD. We then proceed with using TD as a therapeutic agent in tumor associated macrophages by modulating the response of PD-L1. The findings of this work create a base for TD in biological applications such as cancer immunotherapy.

## 1. Introduction

Cancer is an age-old disease with still a lot to unfold. The primary treatment for cancer includes surgery, chemotherapy and radiotherapy. We are now in the transformative era of targeted therapies, immunotherapies and personalized medicine.[1] However, we are still struggling with finding a definitive cure. Cancer forms a complex tumor environment which includes cancer cells, stem cells, immune cells (macrophages, T cells), blood vessels, and extracellular matrix.[2] Tumor microenvironment can promote drug resistance and immune evasion which might present significant challenges in formulating effective treatment strategies.[3] Further advancements in cancer research are essential for deciphering the complexities and developing new and innovative treatments.

Macrophages are important part of our innate immune system.[4] They transition from the resting stage (M0) to the active stage (M1 and M2). M1 macrophages are generally termed as fighters as they defend against pathogens. On the other hand, M2 macrophages act as healers during tissue repair. In diseases such as cancer, macrophages are recruited as anti-cancer moieties. However, in the tumor microenvironment, the cancer cells repolarize the macrophage to pro-tumoral.[5] These macrophages are termed tumor associated macrophages (TAMs). They help the tumor in processes such as angiogenesis, tumor growth, metastasis, and creating an immunosuppressive environment.[6] The current therapies are focused on targeting the cancer cells but not on the entire tumor microenvironment.[7] Targeting TAMs alongside existing therapies could enhance overall improvement in cancer therapy.

DNA nanotechnology is a booming field focused on applications in disease treatment and therapeutic interventions. The principles of DNA nanotechnology utilize the Watson–Crick base pairing principles to design complex nanostructures.[8] Prof. Ned Seeman first formed a 4-way junction marking the start of the field.[9] Since then, various structures such as DNA tetrahedron (TD),[10] DNA icosahedron,[11] DNA cube,[12] and so on have emerged. TD is a nanocage with a plethora of advantages and applications associated with it. It has been used for different applications such as drug delivery,[13–15] stem cell differentiation,[16,17] and gene silencing[18] among others. TD has also shown anti-oxidative and anti-inflammatory activities.[19]

In this study, we explore the potential application of TD in tumor immunology. We synthesized TD and characterized it using various techniques. We first checked the anti-oxidative properties of TD followed by anti-inflammatory properties. We proceeded further by checking the effect of TD on the phagocytosis mechanism in the M0 and activated macrophage cells. We established that TD alone does not cause any immune reaction. So, we further investigated the role of TD in TAMs. Finally, we also explored the targets affected by TD in TAMs. Our study will open up new avenues of TD in the field of immunology which is not yet fully explored.

## 2. Results

### 2.1. Synthesis and characterization of the tetrahedron

We used a one pot synthesis to carry out TD synthesis[20] (Fig. 1a). In brief, the four primers (M1, M2, M3 and M4) were mixed in

*Department of Biological Sciences and Engineering, Indian Institute of Technology Gandhinagar, Palaj 382355, Gujarat, India. E-mail: dhiraj.bhatia@iitgn.ac.in*
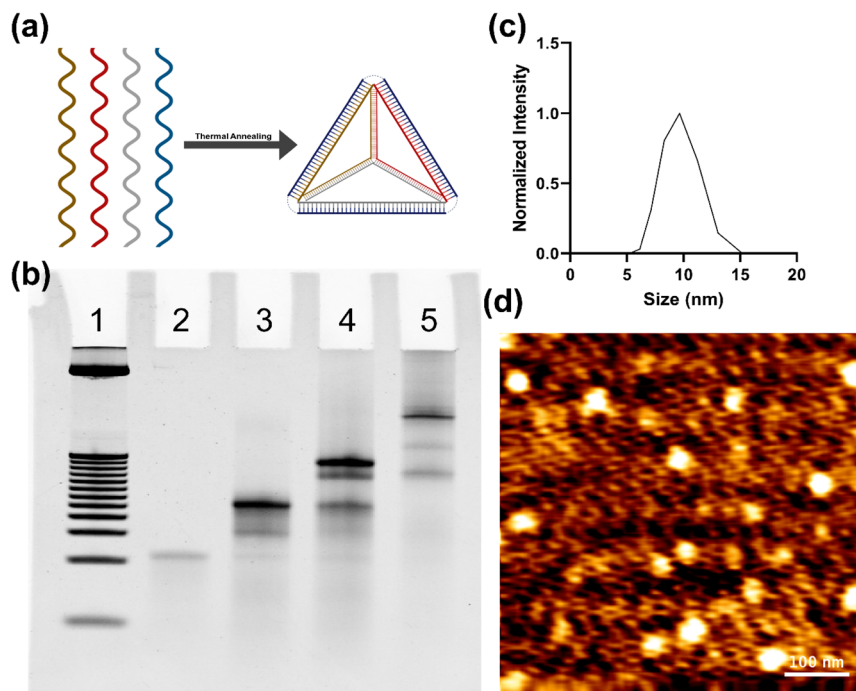
Fig. 1  Synthesis and characterization of the DNA tetrahedron (TD). (a) Schematic representation of TD synthesis. Four single stranded primers are subjected to thermal annealing to form TD. (b) EMSA performed using 8% native PAGE. Lane 1: 25 bp DNA Ladder; Lane 2: M1; Lane 3: M1 + M2; Lane 4: M1 + M2 + M3; Lane 5: M1 + M2 + M3 + M4. Band retardation shows higher order structure formation. (c) DLS showing the hydrodynamic size of TD as 9.2 ± 0.78 nm. (d) AFM image showing the triangular morphology of TD.

an equimolar ratio in 2 mM $MgCl_2$ buffer, followed by thermal annealing. Size and morphology-based characterization of TD was carried out using EMSA, DLS and AFM. The EMSA technique relies on band retardation based on molecular weight. We used 8% native PAGE to check the band pattern when different numbers of primers were added in the same ratio. We found that with increasing number of primers, the migration becomes slow, being the least in TD (Fig. 1b). This shows higher order structure formation. We then moved to check the size of the formed structure using DLS. DLS shows the hydrodynamic size based on light scattering. We found the hydrodynamic size of TD as 9.2 ± 0.78 nm (Fig. 1c). We proceeded to check the morphology of the formed TD using AFM. We found triangular structure formation with size around 18–20 nm (Fig. 1d). We finally carried out the stability assay for TD using serum and found it to be stable up to 2 hours after which it started degrading (ESI Fig. 1†).

## 2.2.  Anti-oxidative and anti-inflammatory properties of the tetrahedron

The levels of reactive oxygen species (ROS) are pivotal for the regulation of various cellular functions.[21] Increased ROS production is the primary inflammatory response in macrophages. We first wanted to establish the effect of TD on ROS and to do that, we used RAW264.7 cells as our macrophage model. It is known that lipopolysaccharide (LPS) can polarize the macrophages to the M1 state and in turn increase the ROS production.[22] So, we divided the cells into 5 groups: non-treated

control, 200 nM TD for 2 hours, 500 ng mL$^{-1}$ LPS for 24 hours, TD pretreatment followed by LPS treatment and post treatment of TD after the LPS treatment. We used DCF-DA for checking the ROS. We found that the level of ROS in the TD treated group is similar to our non-treated cells indicating that TD doesn't have the capability to induce ROS by itself (Fig. 2a and b). LPS treated cells, which acted as our positive control, had the highest levels of ROS. The cells pre-treated and post-treated with TD had decreased levels of ROS compared to LPS. To verify the same, we repeated the same experiment using a multimode plate reader which indicated the same pattern (ESI Fig. 2†). This suggests that TD does have anti-oxidative properties.

Increased expression of HIFα has shown increased levels of ROS.[23] To check whether a similar correlation is applicable to macrophages, we carried out HIFα immunostaining. We found a similar trend in the expression of HIFα to ROS levels, which validated our results (Fig. 2c and d). ROS production is required for IL6 release in M1 macrophages.[24] IL6 is one of the pro-inflammatory cytokines released by M1 macrophages.[25] So, we estimated the levels of IL6 in our treatment groups. We found that in cells treated with LPS, the IL6 levels were the highest (Fig. 2e). With pre- or post-treatment of TD, the levels of IL6 decreased compared to LPS. We also checked for IL10, an anti-inflammatory cytokine (ESI Fig. 3†). We found that the gene expression of IL10 was less in LPS induced cells. However, it increased significantly with pre- or post-treatment of TD in LPS induced cells. Hence, we showed that TD has anti-oxidative and anti-inflammatory properties.
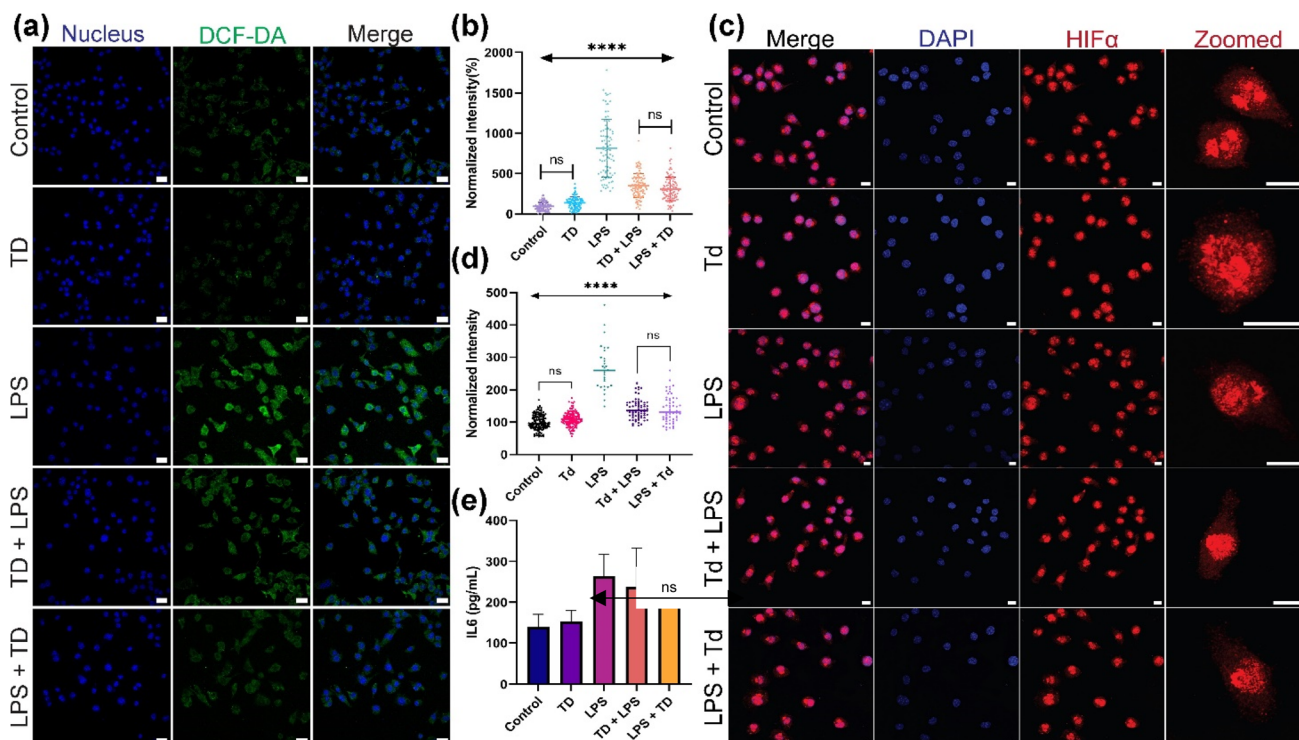
**Fig. 2** Anti-oxidative and anti-inflammatory properties of TD. (a) Confocal images of DCF-DA staining showing ROS levels in RAW264.7 cells. Green color indicates ROS levels by DCF-DA staining and blue color indicates nucleus stained by DAPI. (b) Quantification of ROS levels of the images in panel (a). (c) Confocal images showing HIFα immunostaining. Blue color indicates DAPI staining of nucleus, red staining indicates HIFα. (d) Quantification of HIFα expression in the cells in panel (c). (e) IL6 levels in the five groups using ELISA. Scale bar is 20 μM.

## 2.3. Tetrahedron decreases the phagocytosis

Macrophages are phagocytes and known for their 'bacteria eating' property.[26] To test the effect of our treatment on phagocytosis, we decided to carry out cellular uptake of FITC-dextran 40 kDa. As expected, the uptake of dextran was highest under the LPS conditions (Fig. 3a and b). With the treatment of TD, we observed that dextran uptake lowered suggesting decreased functionality of the macrophages. Since activated macrophages have higher dextran uptake, the decreased phagocytosis with the treatment of TD is indicative of deactivation of macrophages. Another marker of activated macrophages is change in morphological features such as cell size.‡ We calculated the cell area to understand the changes happening by the treatment of TD on LPS activated cells. We found that LPS treated cells had the highest area which decreased on pre- and post-treatment of TD (Fig. 3c). The cell area decrease upon TD treatment supports our hypothesis and gives us confidence to study the role of TD in tumor associated macrophages.[27]

## 2.4. Targeting tumor associated macrophages

With establishing the role of TD in phagocytosis and the anti-oxidative and anti-inflammatory properties, we decided to

explore the effect of TD in TAMs. We treated the RAW264.7 cells with conditioned medium from HeLa cells.[28] The conditioned media was collected from confluent HeLa cells, followed by centrifugation to remove any debris. The RAW264.7 cells were treated with conditioned media for 24 hours. The cytokines and chemokines released from the cancerous cells will polarize the RAW264.7 cells to act like TAMs. We then treated the TAMs with TD to check its effect on ROS levels. We found that TAMs had significantly higher levels of ROS compared to the non-treated control (Fig. 4a and b). The treatment with TD was successful in reducing the levels of ROS. We also checked for the HIFα levels in TAMs and TD treated TAMs. The expression pattern of HIFα was similar to the levels of ROS (ESI Fig. 4†). This suggests that TD can actually be used for effective treatment of TAMs in the tumor microenvironment.

To further validate our findings, we studied the gene expression of NFkB. NFkB is shown to maintain the tumor promoting phenotype of TAMs in certain cancers.[29] NFkB has also been linked to the evolution of inflammatory tumors.[30] In our study, we found that in TAMs, the NFkB was highly upregulated and after TD treatment, NFkB downregulated significantly (Fig. 4c). This confirmed our initial findings of TD as a treatment modality for TAMs.

## 2.5. TD targets PDL1 for depolarizing TAMs

To analyze the underlying mechanism for TD to target TAMs, we decided to take one step further. PD-L1 is found in healthy cells

‡ E. J. Kim, M. Y. Lee, and Y. J. Jeon, Silymarin inhibits morphological changes in LPS-stimulated macrophages by blocking NF-κB pathway, *Korean J. Physiol. Pharmacol.*, **2015**, 19(3), 211–218.
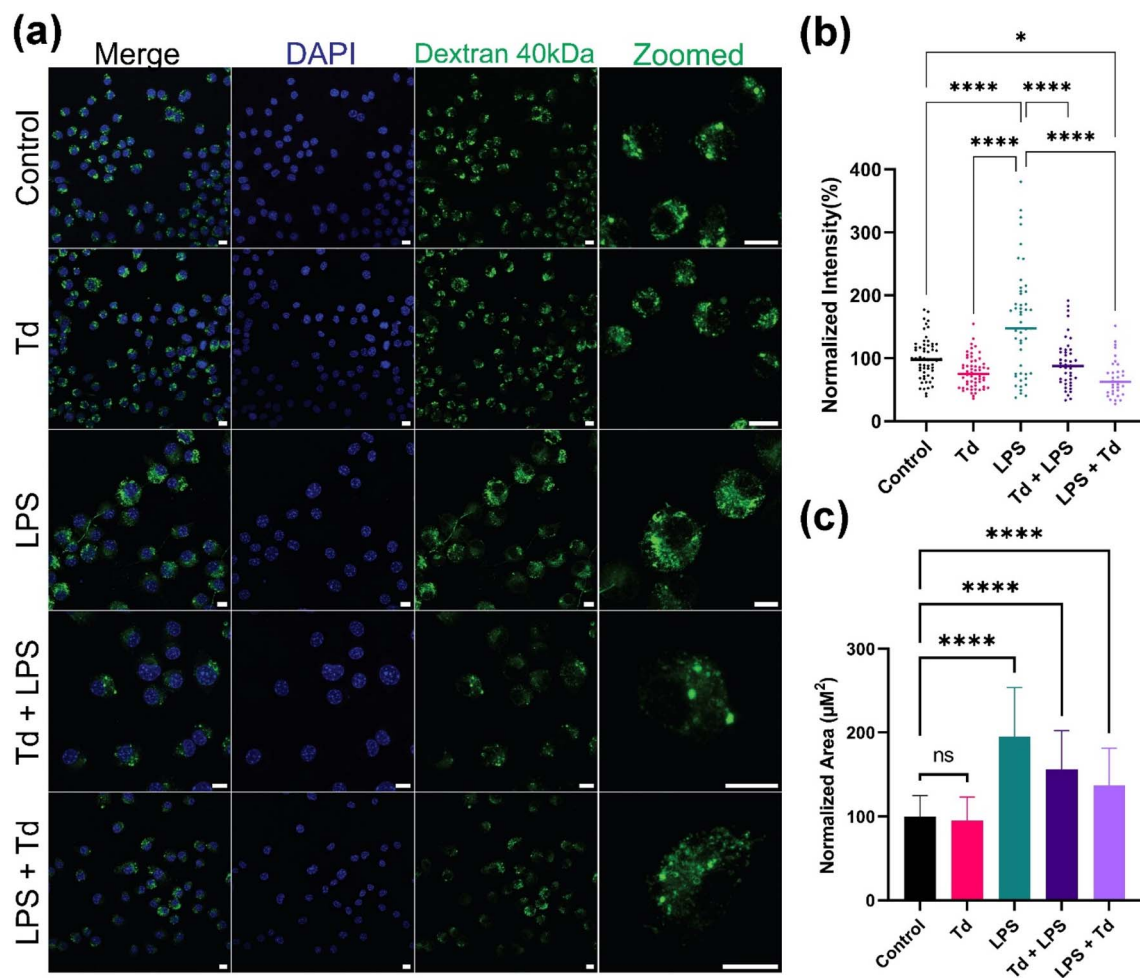
**Fig. 3** Phagocytosis. (a) Confocal images showing cellular uptake of FITC dextran. Blue color indicates DAPI staining of nucleus, green color indicates 40 kDa dextran. (b) Quantification of dextran uptake shown of images in panel (a). (c) The area of cells treated with LPS and TD during phagocytosis. Scale bar is 20 μM.

and sends signals to immune cells, particularly T cells, to not attack them.[31] Cancer cells have a high amount of PD-L1, helping them to escape immune attack.[32] Multiple cytokines released by TAMs can also upregulate the expression of PD-L1 by activation of the JAK/STAT pathway.[33] HIF can also bind to the hypoxia response element of the PD-L1 promoter region and induce the transcription of PD-L1.[34] So, we proceeded with immunostaining of PD-L1 and found the expression of PD-L1 significantly higher in TAMs compared to the control (Fig. 5a and b). When treated with TD, the expression of PD-L1 decreased significantly. PD-L1 undergoes clathrin mediated endocytosis, which is also the route of the entry taken by TD. This might suggest the interaction of TD and PD-L1. HIFα levels are also lowered (ESI Fig. 3†) which further confirm the transcription regulation of PD-L1. We also know that the cell shape indicates the polarity of macrophages.[35] After TD treatment, the cell area of TAMs is decreased (Fig. 5c). This suggests that TD is depolarizing TAMs by downregulating the expression of PD-L1. The efficacy of PD-1 inhibitors is low and modulating the expression of PD-L1 might increase their efficacies.

# 3. Materials and methods

## 3.1. Materials

The primers (M1–M4) were obtained from Sigma Aldrich. Nuclease free water and magnesium chloride were obtained from SRL, India. Acrylamide : bisacrylamide (30%), TEMED, APS, Penstrap, paraformaldehyde, ethidium bromide, and Triton X were obtained from Himedia. 6× loading dye, 25 bp ladder, Mowiol, IL6 ELISA kit, lipopolysaccharides (LPS), DCF-DA, and DAPI were obtained from Sigma Aldrich. Goat anti-rabbit A647 secondary antibody was obtained from Invitrogen. Anti-mouse IgG (H + L) F(ab)2 Fragment (A647) and HIFα antibody were obtained from CST. PD L1 antibody was obtained from eBioscience. DMEM Media, FBS, and trypsin were obtained from Gibco. RNA extraction kit and reverse transcription kit were obtained from Qiagen.

## 3.2. Synthesis of the tetrahedron

DNA tetrahedron was synthesized as described previously. Briefly, four single stranded oligonucleotides (ESI Table 1†)
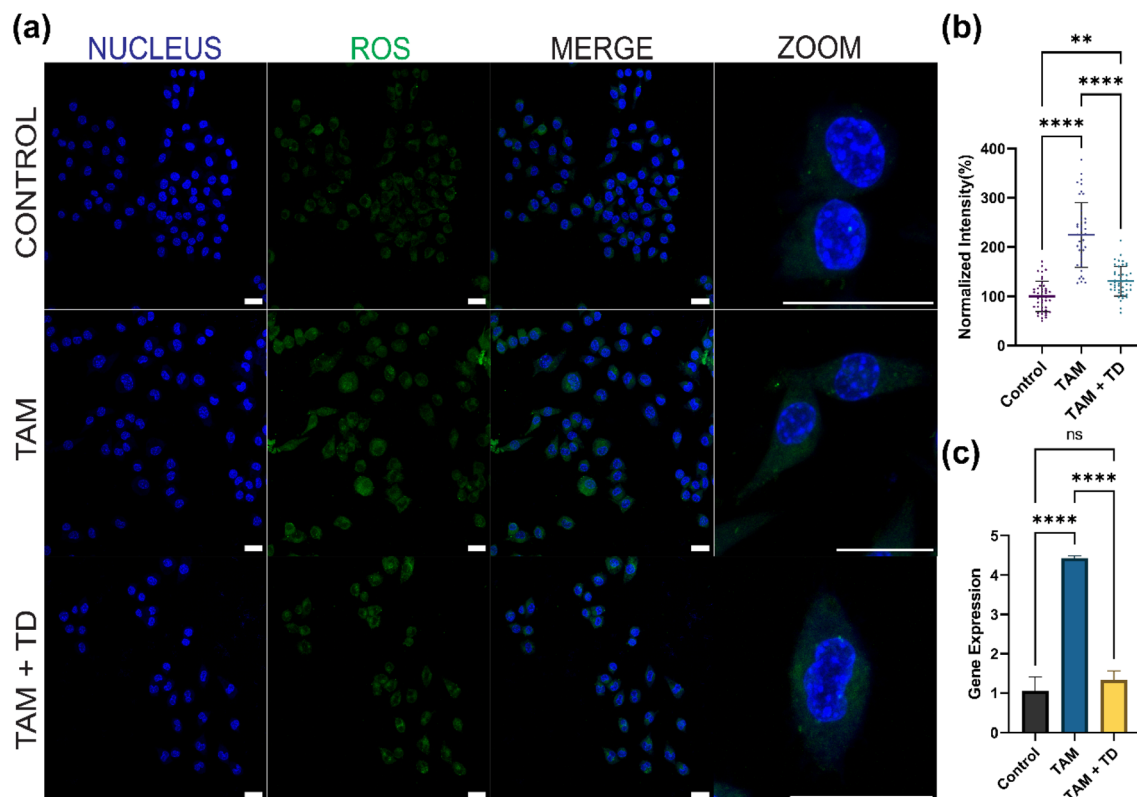
**Fig. 4** Targeting tumor associated macrophages. (a) Confocal images showing ROS levels using DCF–DA staining. Blue color indicates DAPI staining of nucleus, green color indicates ROS levels. (b) Quantification of ROS level shown of images in panel (a). (c) NFkB expression levels using real time PCR. Scale bar is 20 μM.

were taken in equimolar ratio with 2 mM $MgCl_2$ and denatured at 95 °C for 30 minutes. They were annealed by gradually decreasing the temperature by 4 °C up to 4 °C for 15 minutes at each step. The final concentration of the DNA tetrahedron was 2.5 μM.

### 3.3. Characterization of the tetrahedron

**3.3.1. Electrophoretic mobility shift assay (EMSA).** EMSA was performed for confirmation of higher order structure formation. Four tubes were taken each containing equimolar ratio of M1, M1 + M2, M1 + M2 + M3, and M1 + M2 + M3 + M4 respectively. They were synthesized using the same protocol and then subjected to 8% native page at 70 V for 90 minutes. The bands were stained using ethidium bromide. The gel was visualized using a Gel Documentation system (Biorad Chem-iDoc MP Imaging System).

**3.3.2. Dynamic light scattering (DLS).** Size-based characterization was done using DLS. The sample was prepared by diluting TD 20-fold. Then it was subjected to DLS using a Malvern Panalytical Zetasizer Nano ZS instrument and the hydrodynamic size was measured.

**3.3.3. Atomic force microscopy (AFM).** The morphology-based characterization was performed using Bio AFM (Bruker JPK NanoWizard sense+). The sample was prepared in 1 : 10 dilution on a freshly cleaved mica sheet and allowed to dry. Then tapping mode was used to observe the DNA tetrahedron. The image was further processed using JPK software.

**3.3.4. Stability assay.** The stability of the TD was checked using serum stability assay. TD was incubated with 10% FBS at 37 °C for different time points (0, 1, 2, 6 hours). The reaction was stopped by immediately storing the tube at −20 °C. 8% native PAGE was run to check the band intensity at 70 V for 90 minutes. The gel was visualized using a Gel Documentation system (Biorad ChemiDoc MP Imaging System).

### 3.4. Cell culture

RAW264.7 cells were kindly gifted by Dr Ashutosh Kumar. RAW264.7 and HeLa cells were maintained in DMEM medium supplemented with 10% FBS and 1% pen-strap. They were maintained at 37 °C in a humidified incubator and 5% $CO_2$.

**3.4.1. Conditioned media.** HeLa cells were grown to 90% confluency in DMEM complete media. The medium was then collected and centrifuged at 200$g$ for 5 minutes. The supernatant was collected and stored at −20 °C until further use.

**3.4.2. Treatment groups.** For the first part of the study, there were 5 treatment groups: control, 200 nM TD for 2 hours, 500 ng $mL^{-1}$ LPS for 24 hours, 200 nM TD followed by 500 ng $mL^{-1}$ LPS for 24 hours, and 500 ng $mL^{-1}$ LPS for 24 hours followed by 200 nM TD for 2 hours. The second part of the study includes three treatment groups: control, TAM (treated with conditioned media for 24 hours), TAM (treated with conditioned media for 24 hours) followed by treatment with 200 nM TD for 2 hours.
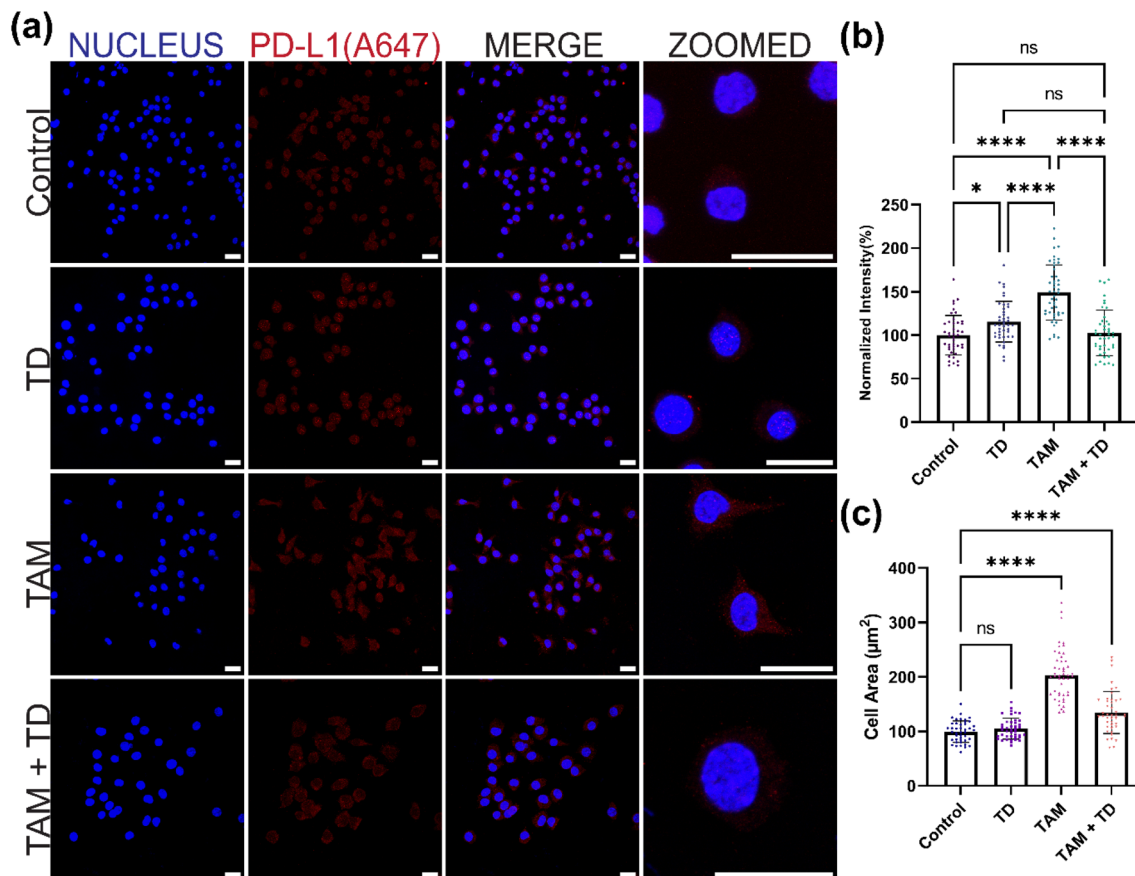
Fig. 5  TD targets PD-L1. (a) Confocal images showing PD-L1 immunostaining. Blue color indicates DAPI staining of nucleus, red color indicates PD-L1 staining. (b) Quantification of PD-L1 level shown of images in panel (a). (c) Cell area of cells shown in panel (a). Scale bar is 20 μM.

## 3.5. Reactive oxygen species (ROS) detection assay by confocal microscopy

ROS was measured using DCF-DA staining. The cells were seeded in a 24 well plate on coverslips and allowed to grow till 80% confluency followed by the treatment. The cells were washed with 1× PBS two times. They were treated with 10 μM DCF-DA for 30 minutes at 37 °C and washed with 1× PBS two times. They were fixed with 4% PFA for 15 minutes at 37 °C, washed three times with 1× PBS and later mounted with DAPI + Mowiol. The slides were stored at 4 °C until imaging.

## 3.6. ROS using a microplate reader

ROS was measured using DCF-DA treatment. The cells were seeded in a 96 well plate and allowed to grow till 80% confluency followed by the treatment. The cells were washed with 1× PBS two times. They were treated with 10 μM DCF-DA for 30 minutes at 37 °C and washed with 1× PBS two times. The 96 well plate was immediately subjected to DCF-DA treatment using a microplate reader (Biotek) and reading was taken at an excitation of 485 nm and emission of 535 nm.

## 3.7. Immunostaining

The cells were seeded in a 24 well plate on coverslips and allowed to grow till 80% confluency followed by the treatment.

They were fixed with 4% PFA for 15 minutes at 37 °C and washed three times with 1× PBS. They were permeabilized with 0.1% Triton-X 100 for 15 minutes at 37 °C and then blocked with a blocking buffer (10% FBS + 0.05% Triton-X 100) for 1 hour at 37 °C. They were subjected to primary antibody treatment at 1 : 100 dilution for 2 hours at 37 °C followed by secondary antibody treatment for 2 hours at 37 °C. The cells were then washed and mounted with DAPI + Mowiol. The slides were stored at 4 °C until imaging.

## 3.8. Cellular uptake

Cellular uptake of dextran 40 kDa was conducted. The cells were seeded in a 24 well plate on coverslips and allowed to grow till 80% confluency followed by the treatment. After the treatment, cells were incubated with 5 mM of 40 kDa dextran for 15 minutes. The cells were washed with 1× PBS two times. They were fixed with 4% PFA for 15 minutes at 37 °C, washed three times with 1× PBS and later mounted with DAPI + Mowiol. The slides were stored at 4 °C until imaging.

## 3.9. ELISA

IL6 levels were measured using an IL6 detection kit (Sigma). The cells were seeded in 6 well plates and treated accordingly. The

supernatant was collected and centrifuged to remove any debris and then further used according to the manufacturer's protocol.

### 3.10. Confocal microscopy

A Leica Sp8 confocal microscope was used for all the imaging. The slides were imaged using a $63\times$ oil immersion objective lens. The pinhole was kept at 1 airy unit. 3 lasers were used to excite different fluorophores; DAPI: 405 nm, Tf-A488, DCFDA, FITC Dextran 40 kDa: 488 nm, and TDCy5, anti-mouse secondary antibody A647, anti-rabbit secondary antibody A647: 633 nm. 4–5 z-stacks were taken for each sample. Image analysis was done using Fiji ImageJ (NIH). The background from each image was subtracted and whole cell intensity was quantified using maximum intensity projection. Minimum 30 cells were quantified to study the cellular experiments.

### 3.11. Quantitative real time PCR

Total RNA was isolated using a Qiagen RNA isolation kit. It was reverse transcribed to cDNA using a Qiagen RT-PCR kit. Target cDNA was amplified using SYBR chemistry (Applied Biosystem) in an Applied Biosystems 7500 system according to the following steps: 55 °C for 2 minutes, 95 °C for 10 minutes, 40 cycles of (95 °C for 30 seconds, 51 °C/55 °C for 1 minute and 72 °C for 1 minute). The melting curve was checked to detect the presence of primer dimers and false priming.

### 3.12. Statistical analysis

All the experiments were carried out in triplicate. The data are presented as mean ± SD. One way ANOVA was carried out with Tukey's correction using GraphPad Prism 9.0. The statistical significance is denoted as follows: * indicates $p \leq 0.05$, ** indicates $p \leq 0.01$, *** indicates $p \leq 0.001$, **** indicates $p \leq 0.0001$, and ns indicates non-significant.

## 4. Conclusions

Our work focused on exploring the capabilities of TD in the aspect of immunology. We found that TD is anti-oxidative and anti-inflammatory and we further explored its role in tumor associated macrophages. To the best of our knowledge, this is the first work exploring the role of TD in tumor associated macrophages. We found that TD can indeed target the tumor associated macrophages by down-regulating the expression of PD-L1. This work will open up the uncharted territory of using TD for not just cancer but also auto-immune diseases. TD treatment can also be explored as preventative medicine. Incorporating TD into cancer immunotherapy has a promising frontier. By targeting TAMs, there is potential to enhance the current therapeutic approaches and pave the way for new treatment modalities.

## Data availability

All the raw data are available from authors upon reasonable request.

## Conflicts of interest

The authors have no conflicts of interest.

## Acknowledgements

## References

1 A. A. Seyhan and C. Carini, Are Innovation and New Technologies in Precision Medicine Paving a New Era in Patients Centric Care?, *J. Transl. Med.*, 2019, **17**(1), 1–28, DOI: **10.1186/S12967-019-1864-9/FIGURES/4**.

2 F. Vahidian, P. H. G. Duijf, E. Safarzadeh, A. Derakhshani, A. Baghbanzadeh and B. Baradaran, Interactions between Cancer Stem Cells, Immune System and Some Environmental Components: Friends or Foes?, *Immunol. Lett.*, 2019, **208**, 19–29, DOI: **10.1016/J.IMLET.2019.03.004**.

3 K. Khalaf, D. Hana, J. T. T. Chou, C. Singh, A. Mackiewicz and M. Kaczmarek, Aspects of the Tumor Microenvironment Involved in Immune Resistance and Drug Resistance, *Front. Immunol.*, 2021, **12**, 656364, DOI: **10.3389/FIMMU.2021.656364/BIBTEX**.

4 S. Yadav, A. Priya, D. R. Borade and R. Agrawal-Rajput, Macrophage Subsets and Their Role: Co-Relation with Colony-Stimulating Factor-1 Receptor and Clinical Relevance, *Immunol. Res.*, 2022, **71**(2), 130–152, DOI: **10.1007/S12026-022-09330-8**.

5 L. Zhou, T. Zhao, R. Zhang, C. Chen and J. Li, New Insights into the Role of Macrophages in Cancer Immunotherapy, *Front. Immunol.*, 2024, **15**, 1381225, DOI: **10.3389/FIMMU.2024.1381225/BIBTEX**.

6 R. Huang, T. Kang and S. Chen, The Role of Tumor-Associated Macrophages in Tumor Immune Evasion, *J. Cancer Res. Clin. Oncol.*, 2024, **150**(5), 1–24, DOI: **10.1007/S00432-024-05777-4**.

7 P. K. T. Wan, A. J. Ryan and L. W. Seymour, Beyond Cancer Cells: Targeting the Tumor Microenvironment with Gene Therapy and Armed Oncolytic Virus, *Mol. Ther.*, 2021, **29**(5), 1668, DOI: **10.1016/J.YMTHE.2021.04.015**.

8 S. Jiang, Z. Ge, S. Mou, H. Yan and C. Fan, Designer DNA Nanostructures for Therapeutics, *Chem*, 2021, **7**(5), 1156–1179, DOI: **10.1016/J.CHEMPR.2020.10.025**.

9 N. C. Seeman, DNA Engineering and Its Application to Nanotechnology, *Trends Biotechnol.*, 1999, **17**(11), 437–443, DOI: **10.1016/S0167-7799(99)01360-8**.

10 R. P. Goodman and A. J. Turberfield, The Single-Step Synthesis of a DNA Tetrahedron, *Chem. Commun.*, 2004, **4**(12), 1372–1373, DOI: **10.1039/B402293A**.

11 D. Bhatia, S. Mehtab, R. Krishnan, S. S. Indi, A. Basu and Y. Krishnan, Icosahedral DNA Nanocapsules by Modular

Assembly, *Angew. Chem., Int. Ed.*, 2009, **48**(23), 4134–4137, DOI: **10.1002/anie.200806000**.

12 J. Chen and N. C. Seeman, Synthesis from DNA of a Molecule with the Connectivity of a Cube, *Nature*, 1991, **350**(6319), 631–633, DOI: **10.1038/350631a0**.

13 P. Vaswani, H. Naveena A, K. Kansara, L. Dahle, A. Kumar and D. Bhatia, DNA Tetrahedron as a Carrier of Doxorubicin for Metastatic Breast Cancer Treatment, *ChemistrySelect*, 2024, **9**(9), e202305222, DOI: **10.1002/slct.202305222**.

14 Z. Xia, P. Wang, X. Liu, T. Liu, Y. Yan, J. Yan, J. Zhong, G. Sun and D. He, Tumor-Penetrating Peptide-Modified DNA Tetrahedron for Targeting Drug Delivery, *Biochemistry*, 2016, **55**(9), 1326–1331, DOI: **10.1021/ACS.BIOCHEM.5B01181/ASSET/IMAGES/LARGE/BI-2015-011812_0006.JPEG**.

15 X. Liu, L. Wu, L. Wang and W. Jiang, A Dual-Targeting DNA Tetrahedron Nanocarrier for Breast Cancer Cell Imaging and Drug Delivery, *Talanta*, 2018, **179**, 356–363, DOI: **10.1016/J.TALANTA.2017.11.034**.

16 W. Ma, X. Shao, D. Zhao, Q. Li, M. Liu, T. Zhou, X. Xie, C. Mao, Y. Zhang and Y. Lin, Self-Assembled Tetrahedral DNA Nanostructures Promote Neural Stem Cell Proliferation and Neuronal Differentiation, *ACS Appl. Mater. Interfaces*, 2018, **10**(9), 7892–7900, DOI: **10.1021/acsami.8b00833**.

17 M. Wei, S. Li, Z. Yang, C. Cheng, T. Li and W. Le, Tetrahedral DNA Nanostructures Functionalized by Multivalent MicroRNA132 Antisense Oligonucleotides Promote the Differentiation of Mouse Embryonic Stem Cells into Dopaminergic Neurons, *Nanomedicine*, 2021, **34**, 102375, DOI: **10.1016/J.NANO.2021.102375**.

18 H. Xue, F. Ding, J. Zhang, Y. Guo, X. Gao, J. Feng, X. Zhu and C. Zhang, DNA Tetrahedron-Based Nanogels for SiRNA Delivery and Gene Silencing, *Chem. Commun.*, 2019, **55**, 4222, DOI: **10.1039/c9cc00175a**.

19 Q. Zhang, S. Lin, S. Shi, T. Zhang, Q. Ma, T. Tian, T. Zhou, X. Cai and Y. Lin, Anti-Inflammatory and Antioxidative Effects of Tetrahedral DNA Nanostructures via the Modulation of Macrophage Responses, *ACS Appl. Mater. Interfaces*, 2018, **10**(4), 3421–3430, DOI: **10.1021/ACSAMI.7B17928**.

20 A. Rajwar, S. R. Shetty, P. Vaswani, V. Morya, A. Barai, S. Sen, M. Sonawane and D. Bhatia, Geometry of a DNA Nanostructure Influences Its Endocytosis: Cellular Study on 2D, 3D, and in Vivo Systems, *ACS Nano*, 2022, **16**(7), 10496–10508, DOI: **10.1021/ACSNANO.2C01382/ASSET/IMAGES/LARGE/NN2C01382_0005.JPEG**.

21 Y. C. Chuang, H. M. Chang, C. Y. Li, Y. Cui, C. L. Lee and C. S. Chen, Reactive Oxygen Species and Inflammatory Responses of Macrophages to Substrates with Physiological Stiffness, *ACS Appl. Mater. Interfaces*, 2020, **12**(43), 48432–48441, DOI: **10.1021/ACSAMI.0C16638/SUPPL_FILE/AM0C16638_SI_001.PDF**.

22 C. Lv, S. Li, J. Zhao, P. Yang and C. Yang, M1 Macrophages Enhance Survival and Invasion of Oral Squamous Cell Carcinoma by Inducing GDF15-Mediated ErbB2 Phosphorylation, *ACS Omega*, 2022, **7**(13), 11405–11414, DOI: **10.1021/ACSOMEGA.2C00571/SUPPL_FILE/AO2C00571_SI_001.PDF**.

23 A. A. Qutub and A. S. Popel, Reactive Oxygen Species Regulate Hypoxia-Inducible Factor $1\alpha$ Differentially in Cancer and Ischemia, *Mol. Cell. Biol.*, 2008, **28**(16), 5106, DOI: **10.1128/MCB.00060-08**.

24 A. M. Franchini, D. Hunt, J. A. Melendez and J. R. Drake, $Fc\gamma R$-Driven Release of IL-6 by Macrophages Requires NOX2-Dependent Production of Reactive Oxygen Species, *J. Biol. Chem.*, 2013, **288**(35), 25098, DOI: **10.1074/JBC.M113.474106**.

25 X. Huang, Y. Li, M. Fu and H. B. Xin, Activating THP1-Derived Macrophage in Vitro, *Methods Mol. Biol.*, 2018, **1784**, 119, DOI: **10.1007/978-1-4939-7837-3_12**.

26 D. Hirayama, T. Iida and H. Nakase, The Phagocytic Function of Macrophage-Enforcing Innate Immunity and Tissue Homeostasis, *Int. J. Mol. Sci.*, 2018, **19**(1), 92, DOI: **10.3390/IJMS19010092**.

27 M. Reyes-López, C. Piña-Vázquez and J. Serrano-Luna, Transferrin: Endocytosis and Cell Signaling in Parasitic Protozoa, *Biomed. Res. Int.*, 2015, **2015**, 641392, DOI: **10.1155/2015/641392**.

28 Y. Zhang, Z. Zhang, L. Chen and X. Zhang, Tumor Cells-Derived Conditioned Medium Induced pro-Tumoral Phenotypes in Macrophages through Calcium-Nuclear Factor $\kappa$B Interaction, *BMC Cancer*, 2022, **22**(1), 1–18, DOI: **10.1186/S12885-022-10431-8/FIGURES/10**.

29 A. Mancino and T. Lawrence, NF-$\kappa$B and Tumor-Associated Macrophages, *Clin. Cancer Res.*, 2010, **16**(3), 784, DOI: **10.1158/1078-0432.CCR-09-1015**.

30 N. Ebrahimi, A. H. R. R. Abdulwahid, A. Mansouri, N. Karimi, R. J. Bostani, S. Beiranvand, S. Adelian, R. Khorram, R. Vafadar, M. R. Hamblin and A. R. Aref, Targeting the NF-$\kappa$B Pathway as a Potential Regulator of Immune Checkpoints in Cancer Immunotherapy, *Cell. Mol. Life Sci.*, 2024, **81**(1), 1–22, DOI: **10.1007/S00018-023-05098-8**.

31 Y. Han, D. Liu and L. Li, PD-1/PD-L1 Pathway: Current Researches in Cancer, *Am. J. Cancer Res.*, 2020, **10**(3), 727.

32 J.-H. Cha, L.-C. Chan, C.-W. Li, J. L. Hsu and M.-C. Hung, Mechanisms Controlling PD-L1 Expression in Cancer, *Mol. Cell*, 2019, **76**(3), 359–370, DOI: **10.1016/j.molcel.2019.09.030**.

33 L. Zhou, T. Zhao, R. Zhang, C. Chen and J. Li, New Insights into the Role of Macrophages in Cancer Immunotherapy, *Front. Immunol.*, 2024, **15**, 1381225, DOI: **10.3389/fimmu.2024.1381225**.

34 M. Z. Noman, G. Desantis, B. Janji, M. Hasmim, S. Karray, P. Dessen, V. Bronte and S. Chouaib, PD-L1 Is a Novel Direct Target of HIF-$1\alpha$, and Its Blockade under Hypoxia Enhanced MDSC-Mediated T Cell Activation, *J. Exp. Med.*, 2014, **211**(5), 781–790, DOI: **10.1084/jem.20131916**.

35 F. Y. McWhorter, T. Wang, P. Nguyen, T. Chung and W. F. Liu, Modulation of Macrophage Phenotype by Cell Shape, *Proc. Natl. Acad. Sci. U. S. A.*, 2013, **110**(43), 17253–17258, DOI: **10.1073/pnas.1308887110**.